ELSEVIER

Chemistry & Biology 8 (2001) 1209–1220

Chemistry & Biology

www.elsevier.com/locate/chembiol

Research Paper

Design and synthesis of a dimeric derivative of RK-682 with increased inhibitory activity against VHR, a dual-specificity ERK phosphatase: implications for the molecular mechanism of the inhibition

Takeo Usui [c], Sachiko Kojima [b], Shun-ichi Kidokoro [b,d], Kazunori Ueda [c], Hiroyuki Osada [c,1], Mikiko Sodeoka [a,b,*]

[a] *Institute of Multidisciplinary Research for Advanced Materials, Tohoku University, Katahira, Aoba, Sendai, Miyagi 980-8577, Japan*
[b] *Sagami Chemical Research Center, Nishi-Ohnuma, Sagamihara, Kanagawa 229-0012, Japan*
[c] *Antibiotics Laboratory, RIKEN, Hirosawa, Wako-shi, Saitama 351-0198, Japan*
[d] *Department of Bioengineering, Nagaoka University of Technology, Kamitomioka-cho, Nagaoka, Niigata 940-2188, Japan*

Received 2 July 2001; revisions requested 30 August 2001; revisions received 21 September 2001; accepted 25 September 2001
First published online 7 November 2001

Abstract

Background: VHR is a dual-specificity phosphatase, which dephosphorylates activated ERK1/2 and weakens the ERK signaling cascade in mammalian cells. A selective inhibitor is expected to be useful for revealing the physiological function of VHR.

Results: First, we investigated the molecular mechanism of VHR inhibition by a known natural product, RK-682. Kinetic analysis indicated that inhibition was competitive toward the substrate, and two molecules of RK-682 were required to inhibit one molecule of VHR. Based on the structure–activity relationships for VHR inhibition by RK-682 derivatives, we constructed a binding model using molecular dynamics calculation. Based on this model, we designed and synthesized a novel dimeric derivative. As expected, the dimeric derivative showed increased inhibition of VHR, supporting our proposed mechanism of VHR inhibition by RK-682.

Conclusion: We have developed a novel inhibitor of VHR based on the results of kinetic analysis and docking simulation.

Keywords: Dual-specificity protein phosphatase; Protein phosphatase inhibitor; RK-682; VHR

1. Introduction

Protein phosphorylation plays critical roles in the control of various cellular functions, such as cell growth, proliferation, oncogenic transformation, and cell cycle progression. The balance of tyrosine phosphorylation is a result of interplay between protein tyrosine phosphatases (PTPs) and protein tyrosine kinases. Perturbation of this balance is thought to be involved in the pathogenesis of cancer and other diseases.

Dual-specificity PTPs (DS-PTPs) are members of a large family of enzymes that catalyze the hydrolysis of phosphomonoester bonds in protein substrates. The DS-PTPs act efficiently on phosphotyrosine as well as phosphothreonine/serine residues [1–3]. Approximately 20 distinct DS-PTPs have been identified to date. The gene of the first identified human DS-PTP, named VHR (vaccinia VH1-related phosphatase), was isolated by an expression cloning strategy and has been the subject of detailed biochemical and structural analyses [4]. DS-PTPs and PTPs share the active site motif (His/Val)Cys(X)$_5$Arg(Ser/Thr), but display little amino acid sequence identity outside of the active site. Reported crystal structures of PTPs and DS-PTPs, including VHR [5], indicate that this motif forms a loop structure, which is thought to interact directly with the phosphate residue of the substrate through multiple hydrogen bondings between amide NH and phosphate

[1] Also corresponding author.

* Corresponding author.
E-mail addresses: antibiot@postman.riken.go.jp (H. Osada), sodeoka@tagen.tohoku.ac.jp (M. Sodeoka).

1074-5521/01/$ – see front matter
PII: S1074-5521(01)00089-8

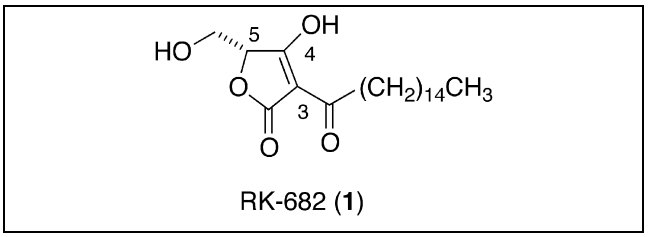

Fig. 1. Structure of RK-682.

oxygen atoms. VHR was recently reported to act as a physiological regulator of ERKs, extracellular regulated kinases, which are members of the MAP (mitogen-activated protein) kinase family [6]. VHR is a constitutively expressed tyrosine-specific ERK phosphatase, localized to the nucleus, and is responsible both for the rapid inactivation of ERK after its activation and for its repression in quiescent cells. Specific inhibitors of VHR are expected be useful for revealing the physiological functions of VHR and also ERK signaling, but only a few VHR inhibitors have been reported so far [7–11]. Since most of them also inhibit other enzymes [7–14], a more selective inhibitor of VHR is required.

To develop a powerful and selective inhibitor of VHR, we focused on a tetronic acid derivative, RK-682 (**1**, see Fig. 1), which had been isolated from *Streptomyces* sp. 88-682 by our group [7] (in this paper we preliminarily reported that **1** was a non-competitive-type inhibitor of VHR, but the experiments described here clearly show that **1** is in fact a competitive inhibitor). We have already synthesized many RK-682 derivatives and clarified the basic structure–activity relationships (SAR) [15–17]. The SAR suggest that highly acidic 3-acyltetronic acid represents a 'core' structure that directly interacts with the active site loop as a phosphate mimic. However, kinetic analysis suggested that the mode of inhibition of VHR by **1** involved two molecules of **1**. In this paper we present details of the kinetic analysis, and we describe the construction of a VHR-RK-682 binding model, and the development of a novel VHR inhibitor based on the binding model.

2. Results and discussion

2.1. Kinetic analysis of VHR inhibition

We evaluated the ability of RK-682 (**1**) to inhibit VHR phosphatase activity, and investigated the mode of inhibition of VHR by **1**. We analyzed the inhibition kinetics of **1** and arsenate, a known competitive PTP inhibitor, on VHR-catalyzed hydrolysis of *p*-nitrophenyl phosphate (pNPP). In each case, a characteristic intersecting line pattern indicating competitive inhibition was observed (Fig. 2A,B). However, the second-order plots showed different patterns (Fig. 2C,D). That for arsenate (Fig. 2D) showed a linear relationship, and the inhibition constant (K_i value) was determined to be 21 μM. In contrast, a quadratic-like curve was observed in the second-order plot for **1** (Fig. 2C). This indicated that two molecules of **1** might bind to and inhibit VHR. Indeed, changing the horizontal axis from [**1**] to $[\mathbf{1}]^2$ resulted in a good linear plot (Fig. 2C, inset). The slight deviation from the line at low $[\mathbf{1}]^2$ might suggest the sequential binding of two molecules of **1** to VHR (see Section 4).

2.2. SARs of RK-682 derivatives

We previously reported the SARs of RK-682 derivatives as inhibitors of VHR, and showed that a free acidic tetronic acid group and a long acyl chain at the C-3 position of **1** are important for the inhibitory activity [17]. These results suggested that both ionic interaction through the dissociated tetronic acid moiety and hydrophobic interaction through the long alkyl chain are important for VHR inhibition. The C-3 ester derivative **2** inhibited VHR with a similar value of IC_{50} (14.5 μM) to that of **1** (11.6 μM), whereas derivatives with a shorter hydrophobic chain showed weaker or no inhibition (**3**: IC_{50} 120 μM, **4**: $IC_{50} > 250$ μM). But the 5-decanoyl derivative of **4** (**5**) did inhibit VHR with a comparable value of IC_{50} (37.2 μM) to that of the 5-decanoyl derivative of **1** (**6**: 37.9 μM). These facts indicate that a long hydrophobic acyl chain at the C-5 position can compensate for a shorter acyl chain at the C-3 position. Since the kinetic analysis suggested that two molecules of **1** are involved, we prepared the simple RK-682 dimer **7**, in which the tetronic acid heads are connected by a C_{22} methylene linker (see Fig. 3). The inhibition profiles of these compounds are compared in Fig. 4A. Although the IC_{50} value (ca. 12 μM) of **7** was similar to that of **1**, the slope of the residual activity curve was very different, suggesting that compound **7** inhibits VHR in a different manner. Indeed, the second-order plot (Fig. 4B) indicated that **7** binds to and inhibits VHR with 1:1 binding stoichiometry. This fact suggests that the second tetronic acid group of **7** might occupy the position of the second RK-682 molecule. Similar slopes to that of **7** were observed for **5** and **6**. These results suggest that compounds **5** and **6** also bind VHR with 1:1 stoichiometry, and the hydrophobic acyl chain at the C-5 position may occupy the site at which the C-3 acyl chain of the second RK-682 molecule binds. It seems probable that the two hydrophobic acyl chains at the C-5 and C-3 positions sit in parallel in the hydrophobic groove near the active site. If this is the case, the methylene linker of the dimer **7** should be tightly folded to fit in the groove, and such conformational restriction may be energetically unfavorable enough to cancel out the favorable interaction between the second tetronic acid group and the enzyme.

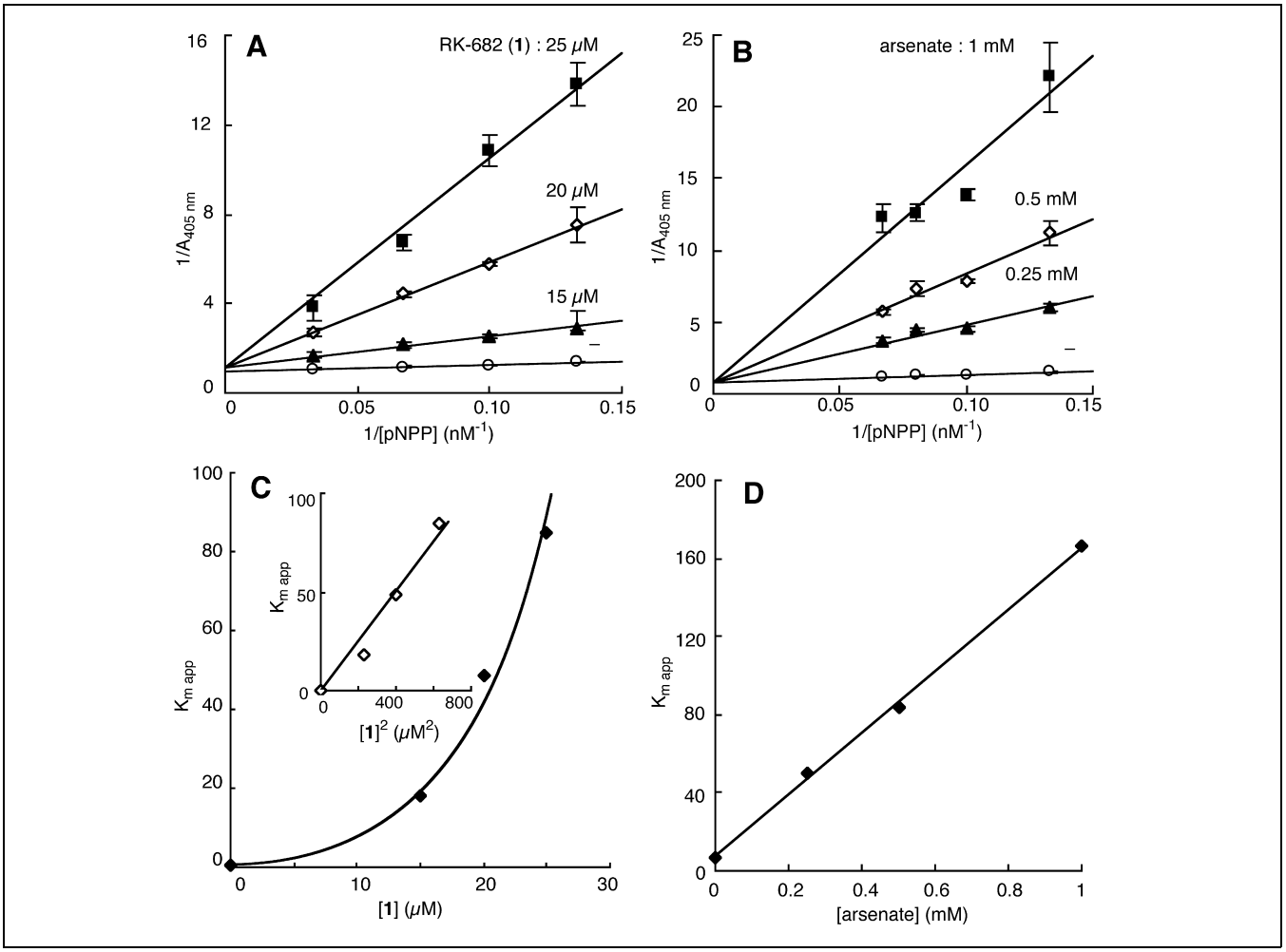

Fig. 2. Effects of compound **1** and arsenate on VHR-catalyzed hydrolysis of pNPP. (A) Lineweaver–Burk plot of the effect of compound **1** on VHR activity. Concentrations of **1** were 0 (○), 15 (▲), 20 (◇), and 25 (■) μM, respectively. (B) Lineweaver–Burk plot of the effect of arsenate on VHR activity. Concentrations of arsenate were 0 (○), 0.25 (▲), 0.5 (◇), and 1 (■) mM, respectively. (C) Second-order plot of (A). The inset shows the second-order plot of (A) with $[\mathbf{1}]^2$ as the horizontal axis. (D) Second-order plot of (B).

2.3. RK-682 binding model for VHR

Based on the findings described above and a reported crystal structure of VHR [5], we constructed a binding model. The hypotheses we used for model building are as follows. (1) The tetronic acid anion of the first molecule binds to the active site loop (Cys124–Arg130) of VHR. The competitive inhibition mode of **1** with respect to the substrate pNPP observed in the kinetic studies and the importance of the acidic free tetronic acid moiety support the idea of a direct interaction between the tetronic acid anion and the catalytic loop structure [17]. (2) The long alkyl chains of the first and second molecules have a hydrophobic interaction with each other and lie in the hydrophobic groove near the active site loop. The SAR and the single-molecule binding mode of the molecules **5** and **6** with a long hydrophobic acyl chain are consistent with this hypothesis. (3) The tetronic acid group of the second molecule has a positive interaction with the basic Arg158 residue of VHR. The guanidino group of Arg158 is located at the bottom of the pocket near the active site loop, and seems to be a good candidate for the putative binding site for the second tetronic acid group. First, the sulfate anion bound to the active site loop in the crystal structure was removed, and the deprotonated RK-682 molecule was manually docked to the active site according to the hypotheses described above. Next, the second RK-682 anion was docked into the Arg158 pocket, and the hydrophobic chains were oriented to the hydrophobic groove. After preliminary optimization using molecular mechanics calculations, energy minimization and analysis of the molecular dynamics in water were carried out using the Amber 4.1 computer package. Based on the final energy-minimized structure, we propose the binding model shown in Fig. 5.

This model contains many positive interactions. The first tetronic acid anion is bound to the active site loop via ionic interaction and/or hydrogen bondings with the Arg130 side chain and the backbone amide NH (Glu126). The second tetronic acid anion interacts with the Arg158

side chain, and hydrogen bonds between the carbonyl oxygen at C-3 position of **1** and amide NH of the active site loop (Gly127 and Tyr128) are also observed. Significant hydrophobic interaction between the two long alkyl chains of the first and second molecules and also between the second chain and hydrophobic amino acid residues of VHR, such as Leu25, are observed.

The interaction between the alkyl chains would be favorable for stable binding to VHR because the hydrophobic groove is too wide for a single alkyl chain.

2.4. Design and synthesis of a dimeric VHR inhibitor

To confirm this binding model, and to develop a more potent and selective inhibitor of VHR, we designed a novel dimeric compound **8**, in which the hydroxymethyl group of the first molecule is connected to the side chain of the second molecule through the appropriate linker (Fig. 5). The dimeric molecule **8** was expected to exist in the appropriate conformation owing to intramolecular hydrophobic interaction, and so should fit in the catalytic groove without significant conformational change upon binding.

Synthesis of **8** is shown in Scheme 1. The linker part having (*S*)-stereochemistry was synthesized from the β-ketoester **9**. Asymmetric hydrogenation using Noyori's catalyst [18] proceeded smoothly to give the desired (*S*)-**10** of 97% ee in 96% yield. Introduction of the hydroxyethyl group was accomplished via successive allylation, ozonolysis and reduction. Following hydrolysis of the ester

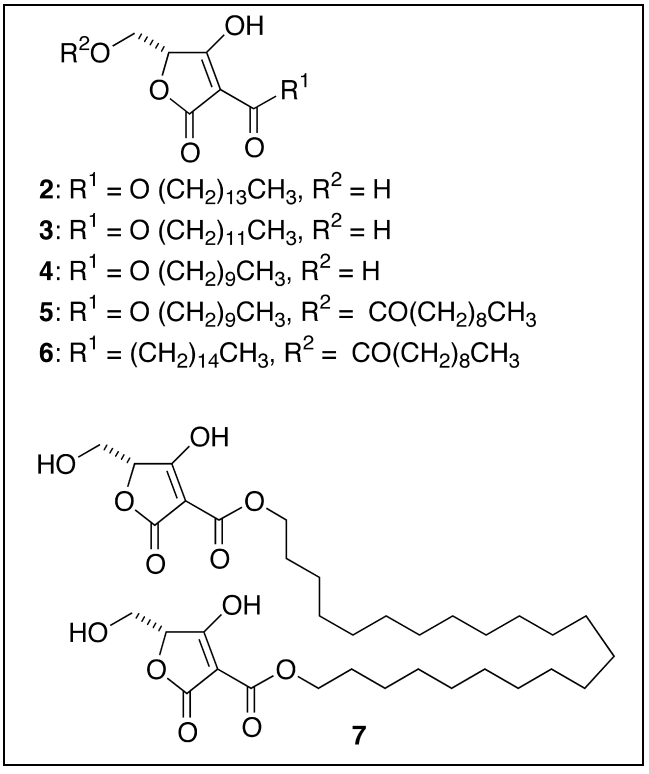

Fig. 3. Structures of compounds **2**–**7**.

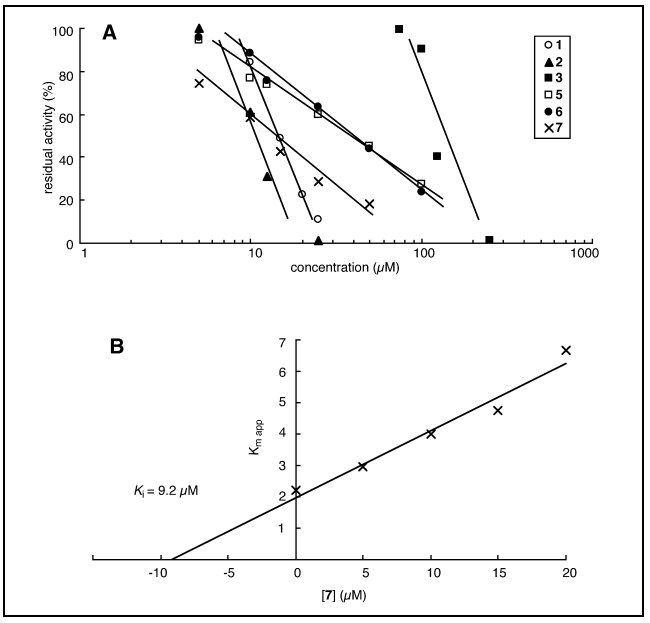

Fig. 4. Inhibition of VHR by tetronic acid derivatives. (A) Concentration-dependent inhibition of VHR by compounds **1**, **2**, **3**, **5**, **6**, and **7**. (B) Second-order plot for **7**.

group, silylation, and selective removal of the silyl ester afforded **11**. After conversion to the acid chloride, the carboxylic acid **11** was then condensed with **1** to give **12** in good yield. The resulting **12** was converted to the alcohol **13**, and the coupling reaction with **14** was achieved in the presence of silver salt. The optically active thioester **14** was prepared according to the procedure reported before [15,16]. The desired product **15** and the detritylated product **16** were obtained in good combined yield. Each compound was treated with tetra-*n*-butylammonium fluoride (TBAF) to construct the tetronic acid moiety, and in the case of **15**, further with hydrochloric acid to afford the desired compound **8**.

*2.5. Increased inhibition of VHR by the dimeric molecule **8***

As expected, compound **8** showed much more potent inhibition of VHR than **1** (Fig. 6A; IC_{50} value of **8** was 1.83 μM), and it showed a competitive/non-competitive mixed-type inhibition pattern (Fig. 6B). The second-order plot showed a linear relationship, not a quadratic-like curve (Fig. 6C), indicating involvement of a single molecule in the inhibition. The synthetic intermediates **13** and **15** without the second tetronic acid group were also tested. The IC_{50} values of **13** and **15** were 10.7 μM and 12.3 μM, respectively, which are similar to that of **1**, but much larger than that of **8**. Since the slope of the residual activity curve of **13** was similar to that of **8** (Fig. 6A), the binding mode of **13** should be similar to that of **8**, i.e., single-molecule binding. These facts are consistent with the proposed critical contribution of the interaction between Arg158 of VHR and tetronic acid anion to strong binding.

The corresponding Arg residue is conserved in many

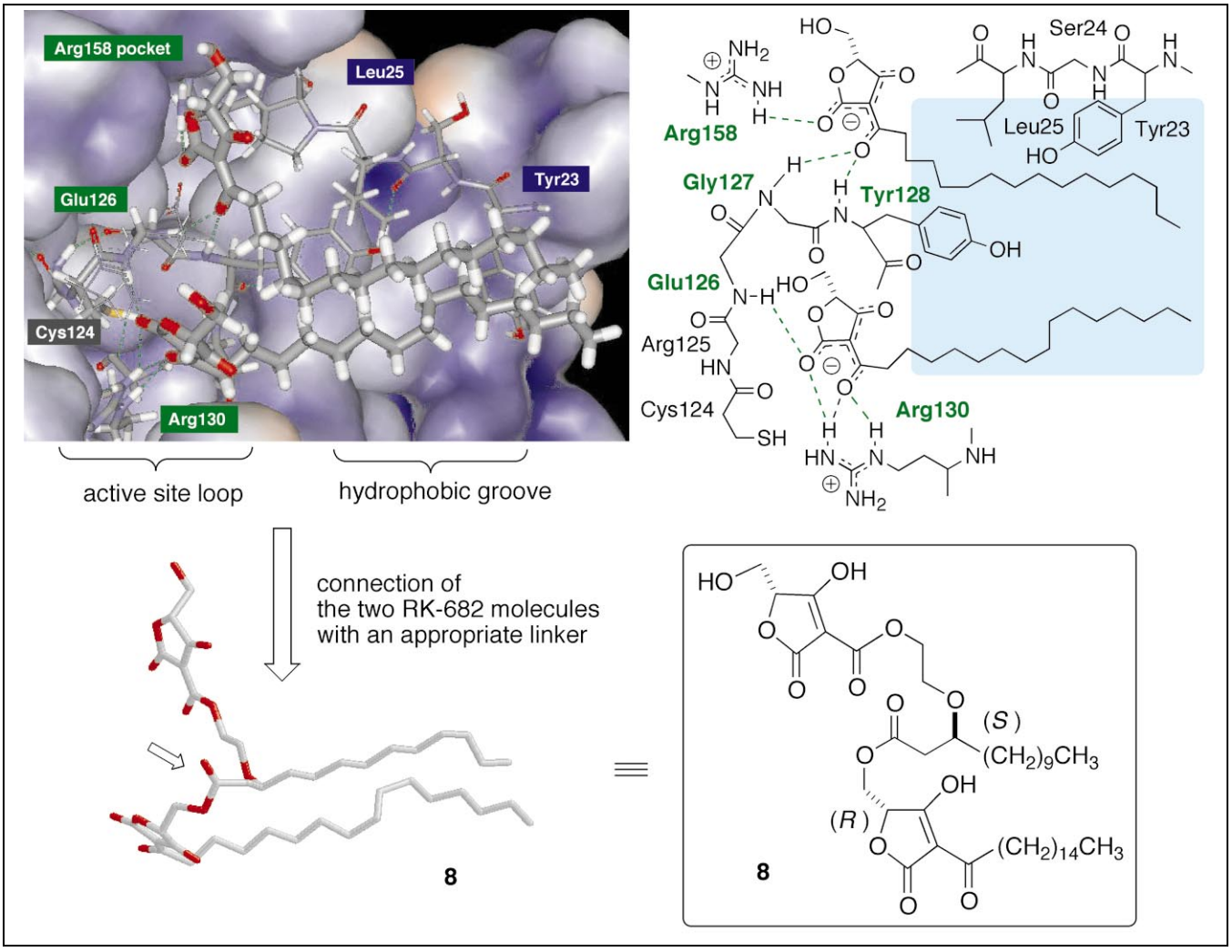

Fig. 5. Proposed binding model of VHR-(RK-682)$_2$ complex and design of a dimeric molecule **8** based on this model.

PTPs, but its environment is different for each enzyme. For example, the corresponding Arg440 in *Yersinia* PTP and Arg257 in PTP1B are buried and no similar charged pocket is observed. In some PTPs there is no corresponding Arg residue (for example, Cdc25A). Recently, Puius et al. reported that PTP1B possesses a non-catalytic aryl phosphate binding site adjacent to its active site, where bis-(*p*-phosphophenyl)methane (BPPM) binds [19,20]. In the reported crystal structure, the aryl phosphate moiety of BPPM interacts with Arg24 and Arg254, both of which are different from the Arg257 corresponding to Arg158 of VHR. These features suggested the possibility that compound **8** would discriminate VHR from other PTPs. To test this possibility, we preliminarily examined the inhibitory activity of **8** for PTP-S2 [21], though the environment of the corresponding Arg residue of this enzyme is still unknown. As expected, **8** did not inhibit PTP-S2 at concentrations up to 100 μM. Since there are many PTP family enzymes, many more PTPs should be tested to evaluate fully the selectivity of **8**. Nevertheless, it is clear that **8** has at least some selectivity to VHR, and suggests a guiding principle for designing selective inhibitors of VHR.

In addition to the previously described SAR data for compounds **2**–**7**, all of these results obtained with the designed molecule **8** strongly support our model for the VHR-(RK-682)$_2$ complex.

3. Significance

We clarified the molecular mechanism of VHR inhibition by RK-682 using kinetic analysis and SAR data of RK-682 derivatives. We constructed a model of the VHR-(RK-682)$_2$ complex with the aid of molecular dynamics calculations. A novel dimeric molecule **8** was designed based on the model, and synthesized. The designed molecule **8** showed highly potent inhibition of VHR, as expected, supporting the validity of our model.

Without the crystal structure of the enzyme–inhibitor complex, it is not easy to know how the compound inhibits the enzyme. Approaches such as kinetic analysis, mo-

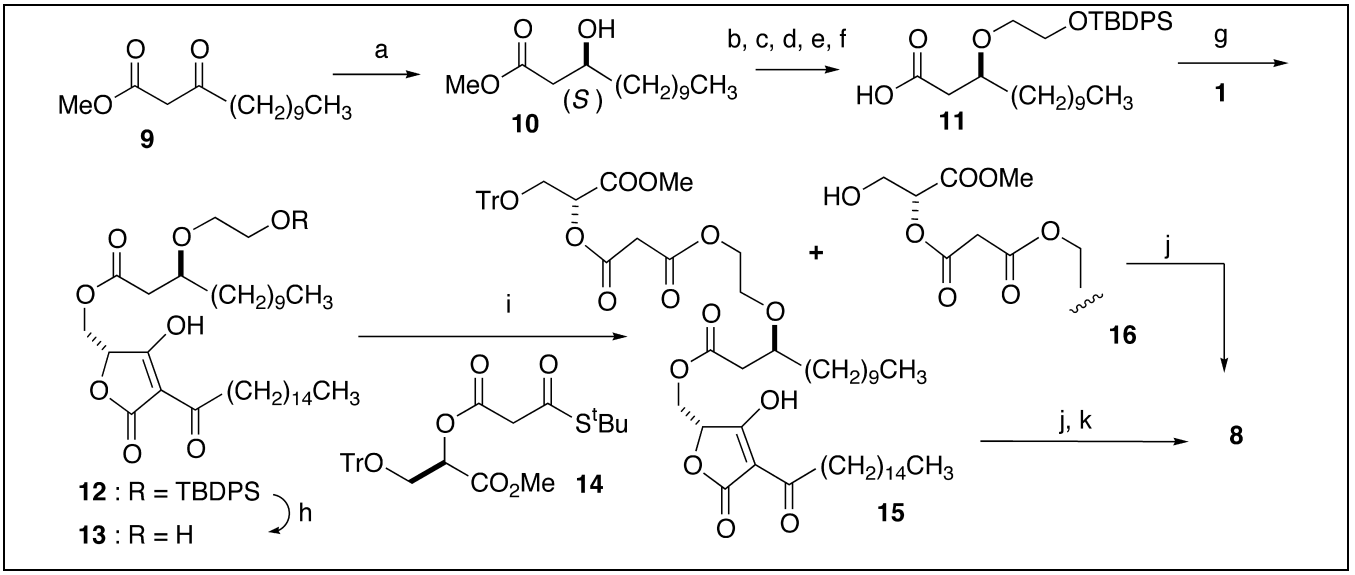

Scheme 1. Synthesis of **8**. (a) Cat. $[RuCl_2((S)\text{-binap})]_2 \bullet NEt_3$, HCl, H_2 (5 atm), MeOH, 60°C, 96% (97% ee); (b) cat. dppb-$Pd_2(dba)_3 \bullet CHCl_3$, $CH_2=CHCH_2OCOOEt$, THF, 65°C, 66%; (c) O_3, MeOH, −60°C, then $NaBH_4$, MeOH, 93%; (d) 1 N NaOH, MeOH, room temperature (rt), 98%; (e) TBDPSCl, imidazole, DMF, rt, 92%; (f) THF–MeOH–H_2O, K_2CO_3, rt, 93%; (g) $(COCl)_2$, DMF, CH_2Cl_2, rt, then **1**, pyridine, CH_2Cl_2, rt, 89%; h) TBAF, THF, 73%; (i) **14**, CF_3COOAg, Na_2HPO_4, benzene, reflux, 60% (**15**)+∼40% (**16**); (j) TBAF, THF, 69% (from **16**); k) 1 N HCl, MeOH, 60% (from **15**, two steps).

lecular modeling, and SAR studies have all been used, but a single approach is rarely effective. The example described in this manuscript indicates that the combination of kinetic analysis, molecular modeling and design, and synthesis of a designed molecule, is a powerful approach for solving this problem. Once a reasonable model is in hand, it should suggest ways to design better inhibitors. In the case of VHR, our model suggests a critical role of the Arg158 pocket for strong binding and subtype selectivity. This finding should be useful for the development of more powerful and selective VHR inhibitors. Studies along this line are under way.

4. Materials and methods

4.1. Overexpression and purification of VHR

The coding sequence for VHR was amplified using PCR from a GST (glutathione *S*-transferase)–VHR fusion gene [4]. The 5′ PCR primer contained an adapter sequence for the DNA restriction enzyme *Nde*I, and the 3′ primer contained a *Bam*HI site downstream of the native stop codon. The PCR product was cloned in the pET3a plasmid (Stratagene) to create pET3a-VHR. The plasmid pET3a-VHR was used to transform competent *Escherichia coli* BL21 (DE3) cells. A transformant harboring this plasmid was grown in 1 l of LB medium containing ampicillin. When the optical density at 600 nm of the culture reached 0.8, IPTG (isopropyl-β-D-thiogalactopyranoside) was added at 1 mM, and incubation of the culture was continued for an additional 8 h. Purification of the overexpressed VHR was performed as previously described [22] with some modifications. The cells were harvested by centrifugation at 5000×*g*, and resuspended in 15 ml of 50 mM Tris (pH 7.4), 1 mM EDTA (ethylenediamine-*N,N,N′,N′*-tetraacetic acid), 1 mM DTT (dithiothreitol), 1% Nonidet P-40, 1 mM PMSF, and lysed by sonication (10 s×6, at output 8, UR-200P, Tomy Seiko Co. Ltd., Tokyo, Japan). The cell debris was removed by centrifugation at 17 000×*g* for 10 min. Ammonium sulfate was added to the cleared cell lysate at 35% saturation and the solution was stirred for 15 min. Thereafter, the precipitate was removed by centrifugation at 17 000×*g*, 20 min, ammonium sulfate was added to the supernatant to 65% saturation, and the solution was stirred, and centrifuged. The resulting pellet was dissolved in a minimum volume of buffer consisting of 50 mM Tris (pH 7.4), 1 mM EDTA, 1 mM DTT, 1 M NaCl, and loaded onto a Sephadex G-75 gel filtration column (Amersham Pharmacia Biotech). After elution with the same buffer, the fractions exhibiting phosphatase activity with pNPP as the substrates were pooled and dialyzed against 500 ml of MES buffer consisting of 20 mM MES (2-(*N*-morpholino)ethanesulfonic acid) (pH 6.0), 1 mM EDTA, 1 mM DTT for 120 min, three times. The dialysate was loaded onto a POROS SP cation-exchange column (4.6×100 mm; Perseptive Biosystems) pre-equilibrated with MES buffer. The column was then washed with MES buffer, and the enzyme was eluted with a 0–250 mM linear NaCl gradient. Fractions containing high phosphatase activity with pNPP as the substrate were analyzed by SDS–PAGE to assess the purity of the enzyme. All fractions which contained only a single band corresponding to VHR were pooled and concentrated by filtration to a final concentration of 0.2 mM. The enzyme was stored at −80°C in 50 mM Tris (pH 7.4), 1 mM EDTA, until use.

4.2. Phosphatase assays

All enzyme assays were performed using pNPP as the substrate at 37°C in 50 mM succinate, 1 mM EDTA, 150 mM NaCl, pH

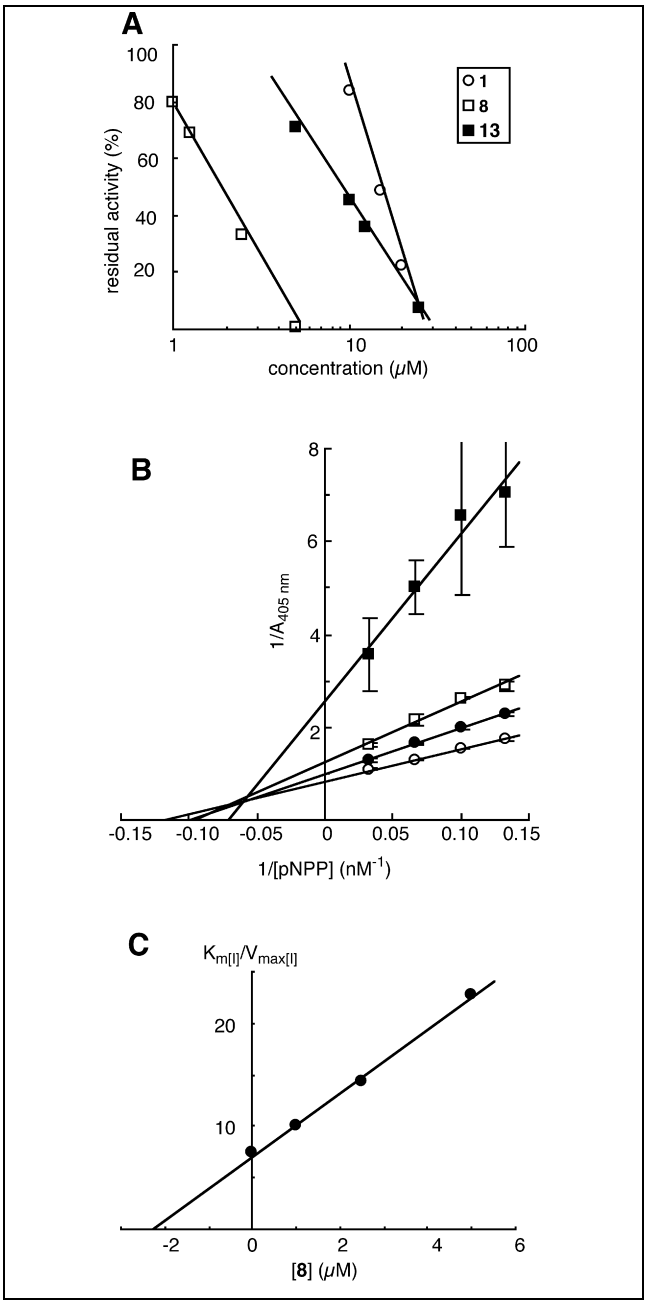

Fig. 6. Effects of compounds **8** and **13** on VHR-catalyzed hydrolysis of pNPP. (A) Concentration-dependent inhibition of VHR by compounds **1** (○), **8** (□), and **13** (■). (B) Lineweaver–Burk plot of the effect of **8** on VHR activity. Concentrations of **8** were 0 (○), 1.25 (●), 2.5 (□), and 5.0 (■) μM, respectively. (C) Second-order plot of (B).

6.0. Immediately after mixing the VHR and pNPP, the reaction mixture (200 μl) was incubated at 37°C for 3 min, then the phosphatase reaction was terminated by adding 1 ml of 1 N NaOH. Phosphatase activity was measured by monitoring the change in absorbance at 405 nm. PTP-S2 assays were carried out according to the reported procedure [23].

For steady-state kinetic analysis, phosphatase activity was measured under conditions in which the pNPP concentration was varied at fixed concentrations of arsenate (Na_2HAsO_4) and compounds **1**–**8**.

The data obtained were fitted to Eq. 1, the Lineweaver–Burk double-reciprocal form based on the Michaelis–Menten equation:

$$1/v = (1 + K_m/[S])/V_{max} \quad (1)$$

The second-order plot is based on Eq. 2, where $K_{m\,app}$, the apparent K_m value, represents the K_m value when $1/v = 0$.

$$K_{m\,app} = K_m\,(1 + [I]/K_i) \quad (2)$$

When binding of two inhibitor molecules is required for inhibition to occur, Eqs. 3 and 4 containing the parameter $[I]^2$ can be derived from Eq. 2. In the case of sequential binding of inhibitor molecules to the enzyme, Eq. 3 is applicable, and when the two inhibitor molecules form a dimer before binding to the enzyme, Eq. 4 is applicable. K_{i1} and K_{i2} represent the first and second inhibitor binding constants, respectively. K_{id} and K_{ib} represent the dimerization constant and the enzyme binding constant, respectively.

$$K_{m\,app} = K_m\,(1 + [I]^2/K_{i1}K_{i2} + [I]/K_{i1}) \quad (3)$$

$$K_{m\,app} = K_m\,(1 + [I]^2/K_{ib}K_{id}) \quad (4)$$

4.3. General methods for the synthesis

Infrared (IR) spectra were measured on an FT/IR-5300 spectrometer. ^{1}H- and ^{13}C-NMR spectra were recorded with a Brucker AM-400, AC-200P, or AVANCE 500 NMR spectrometer with tetramethylsilane used as an internal standard. Mass spectra (MS) were obtained with a Hitachi M-80B mass spectrometer using an electronic ionization method, unless mentioned otherwise. Secondary ion mass spectra (SIMS) were obtained with a Hitachi M-80A mass spectrometer. FAB-MS were measured on a JEOL JMS-HX110 double-focusing mass spectrometer. Optical rotation was measured on a Horiba SEPA-200 polarimeter. In general, reactions carried out under anhydrous conditions utilized in dry solvents under argon atmosphere.

4.4. 3,3′-Docosamethylenedioxycarbonyl-bis[5(R)-hydroxymethytetronic acid] (7)

To a solution of **14** (200 mg, 0.384 mmol) in THF (3.0 ml) were added 1,22-docosanediol (32.8 mg, 0.0957 mmol) and silver trifluoroacetate (213 mg, 0.962 mmol), and the mixture was stirred at 23°C for 3 h while shielded from light. The mixture was diluted with ether, passed through a short silica gel column, and concentrated. The residue was purified by silica gel column chromatography (hexane-AcOEt, 10:1–5:1) to give 1,22-bis{3-[1(*R*)-methoxycarbonyl-2-triphenylmethyloxyethyl]oxy-3-oxopropanoyloxy}-docosane (72.7 mg, 63%) as a colorless oil.

^{1}H-NMR ($CDCl_3$, 500 MHz) δ 1.27 (m, 36H), 1.61 (m, 4H), 3.49 (d, $J = 4.1$ Hz, 4H), 3.52 (d, $J = 16.3$ Hz, 2H), 3.54 (d, $J = 16.3$ Hz, 2H), 3.73 (s, 6H), 4.13 (t, $J = 7.1$ Hz, 4H), 5.27 (t, $J = 4.1$ Hz, 2H), 7.20–7.35 (m, 18H), 7.41 (d, $J = 7.5$ Hz, 12H); IR (neat) 2920, 2850, 1755, 1735, 1445, 1210, 705 cm^{-1}; SIMS *m/z* 1225 (M^++Na).

To a solution of 1,22-bis{3-[1(*R*)-methoxycarbonyl-2-triphenylmethyloxyethyl]oxy-3-oxopropanoyloxy}docosane (72.7 mg, 0.0604 mmol) in THF (0.9 ml) was added TBAF (1 M THF solution, 0.18 ml, 0.18 mmol), and the mixture was stirred at 23°C for 3 h. After the second addition of TBAF (0.18 ml, 0.18 mmol), the mixture was further stirred for 16.5 h at 23°C.

The reaction mixture was quenched by the addition of 1 N aqueous HCl and poured into ice-water; the mixture was then extracted with $CHCl_3$. The organic layer was washed with brine, dried (Na_2SO_4), and concentrated. The residue was purified by silica gel column chromatography ($CHCl_3$–MeOH, 20:1–10:1) to give crude 3,3′-docosamethylenedioxycarbonyl-bis[5(*R*)-triphenylmethyloxymethytetronic acid] as a yellow solid. This material was dissolved in a mixture of methanol (4.0 ml) and $CHCl_3$ (1.0 ml), and 1 N aqueous HCl (0.12 ml, 0.12 mmol) was added to the solution. The mixture was stirred at 23°C for 16.5 h. After removal of the solvent in vacuo, the residue was purified by silica gel column chromatography ($CHCl_3$–MeOH, 1:0–3:1). The combined and concentrated fractions containing the desired product were redissolved in $CHCl_3$, washed with 0.5 N aqueous HCl and water, dried (Na_2SO_4), and concentrated to give **7** (16.0 mg, 40%) as a colorless solid.

^{1}H-NMR (DMSO-d_6, 500 MHz) δ 1.27 (m, 36H), 1.54 (m, 4H), 3.57 (dd, J = 12, 4.3 Hz, 2H), 3.71 (dd, J = 12, 2.4 Hz, 2H), 3.99 (t, J = 6.5 Hz, 4H), 4.66 (m, 2H); IR (KBr) 3420, 2920, 2850, 1715, 1600, 1455, 1055 cm^{-1}; FABMS (+NaCl) *m/z* 655 (M^++H), 677 (M^++Na); HR-FABMS (+NaCl) (M^+-2H+3Na) calculated for $C_{34}H_{52}O_{12}Na_3$: 721.3152, found 721.3105; mp 140°C (dec.).

4.5. Methyl 3-oxo-tridecanoate (*9*)

To a solution of undecanoic acid (2.79 g, 15.0 mmol) in THF (180 ml) was added *N,N′*-carbonyldiimidazole (CDI) (4.86 g, 30.0 mmol), and the mixture was stirred at 23°C for 3 h. To this mixture malonic acid monomethyl ester magnesium salt (9.10 g, 30.0 mmol) was added, and the mixture was stirred at 23°C for 20 h. After further addition of the magnesium salt (910 mg, 3.00 mmol) and stirring at 23°C for 23 h, the reaction was quenched by the addition of saturated aqueous NH_4Cl, and the mixture was then extracted with AcOEt. The organic layer was washed with saturated aqueous NH_4Cl and brine, dried (Na_2SO_4), and concentrated. The residue was purified by silica gel column chromatography (hexane-AcOEt, 50:1–20:1) to give **9** (3.46 g, 95%) as a colorless oil.

^{1}H-NMR ($CDCl_3$, 200 MHz) δ 0.88 (t, J = 6.9 Hz, 3H), 1.26 (m, 14H), 1.58 (m, 2H), 2.19 (t, J = 7.6 Hz, 2/6H), 2.53 (t, J = 7.4 Hz, 10/6H), 3.45 (s, 10/6H), 3.73 (s, 3/6H), 3.74 (s, 15/6H), 4.99 (s, 1/6H), 12.02 (s, 1/6H); ^{13}C-NMR ($CDCl_3$, 125 MHz) δ 14.05, 22.63, 23.45, 28.97, 29.25, 29.31, 29.40, 29.50, 31.84, 43.04, 48.98, 52.25, 167.65, 202.77; IR (neat) 2930, 2860, 1755, 1720, 1240 cm^{-1}. MS *m/z* 242 (M^+), 169, 129, 116 (bp); Anal. Calculated for $C_{14}H_{26}O_3$: C, 69.38; H, 10.81. Found: C, 68.38; H, 10.60.

4.6. Methyl (*S*)-3-hydroxytridecanoate (*10*)

To a degassed solution of **9** (576.8 mg, 2.38 mmol) in methanol (0.8 ml) were added 2 N aqueous HCl (1.5 μl, 0.1 mol%) and dichloro[(*S*)-(−)-2,2′-bis(diphenylphosphino)-1,1′-binaphthyl]ruthenium (II) dimer triethylamine adduct (1.9 mg, 0.05 mol%). After degassing by five freeze–pump–thaw cycles the mixture was transferred to an autoclave, and stirred at 60°C under hydrogen (5 atm) for 20 h. After addition of hexane, the resulting precipitate was removed by filtration, and the filtrate was concentrated. The residue was purified by silica gel column chromatography (hexane-AcOEt, 10:1) to give **10** (553.3 mg, 96%, 97% ee) as a colorless solid.

^{1}H-NMR ($CDCl_3$, 500 MHz) δ 0.88 (t, J = 7.0 Hz, 3H), 1.26 (m, 15H), 1.43 (m, 2H), 1.52 (m, 1H), 2.41 (dd, J = 9.0, 16.4 Hz, 1H), 2.51 (dd, J = 3.4, 16.4 Hz, 1H), 2.81 (d, J = 4.1 Hz, 1H), 3.71 (s, 3H), 4.00 (m, 1H); ^{13}C-NMR ($CDCl_3$, 125 MHz) δ 14.06, 22.64, 25.45, 29.29, 29.49, 29.52, 29.55, 29.57, 31.87, 36.54, 41.12, 51.66, 68.01, 173.44; IR (neat) 3540, 2920, 2850, 1720, 1205, 1180 cm^{-1}; MS *m/z* 244 (M^+), 226 (M^+-H_2O), 103 (bp); CIMS (isobutane): 245 (M^++H), 227 (M^+-OH); HRMS (M^+) calculated for $C_{14}H_{28}O_3$: 244.2037. Found 244.2037.

$[\alpha]_D^{20}$+15.12° (*c* 0.655, $CHCl_3$); mp 37°C.

The ee of the product was determined by the NMR analysis (in $CDCl_3$) of its α-methoxy-α-trifluoromethylphenylacetyl (MTPA) ester. Briefly, **10** was treated with (*S*)-(+)-MTPA chloride (1.5 eq) and pyridine (10 eq) in CH_2Cl_2 at 0°C for 17 h to give the MTPA ester in 98% yield. The racemic **10** prepared by the reduction of **9** with sodium borohydride was similarly converted to its MTPA ester using (*S*)-MTPA chloride. Enantiomeric excess was determined from the integration values of singlets at 3.59 ppm and 3.66 ppm due to the ester methyl group of the (*S*)- and (*R*)-isomer, respectively.

4.7. Methyl (*S*)-3-allyloxytridecanoate

To a stirred solution of tris(dibenzylideneacetone)dipalladium complex ($Pd_2(dba)_3$•$CHCl_3$), (127.8 mg, 0.123 mmol) and 1,4-bis(diphenylphosphino)butane (dppb) (210.1 mg, 0.493 mmol) in degassed THF were added **10** (1.20 g, 4.91 mmol) and allyl ethyl carbonate (2.60 ml, 19.8 mmol), and the mixture was stirred at 60∼65°C for 9 h with bubbling of argon to remove CO_2. After removal of the solvent, the residue was purified by silica gel column chromatography (hexane-AcOEt, 50:1–20:1) to give methyl (*S*)-3-allyloxytridecanoate (916.8 mg, 66%) as a pale yellow oil.

^{1}H-NMR ($CDCl_3$, 500 MHz) δ 0.88 (t, J = 6.9 Hz, 3H), 1.33 (m, 16H), 1.53 (m, 2H), 2.44 (dd, J = 5.4, 15.1 Hz, 1H), 2.56 (dd, J = 7.3, 15.1 Hz, 1H), 3.68 (s, 3H), 3.78 (m, 1H), 4.01 (d, J = 5.6 Hz, 2H), 5.14 (dd, J = 1.6, 10.4 Hz, 1H), 5.25 (dd, 1.6, 17.2 Hz, 1H), 5.89 (tdd, J = 5.6, 10.4, 17.2 Hz, 1H); ^{13}C-NMR ($CDCl_3$, 125 MHz) δ 14.07, 22.65, 25.15, 29.30, 29.53, 29.56, 29.58, 29.61, 31.88, 34.44, 39.77, 51.53, 70.45, 75.89, 116.61, 135.09, 172.24; IR (neat) 2940, 2860, 1745, 1440, 1090, 925 cm^{-1}; MS *m/z* 253 (M^+-OMe), 243 (M^+-$CH_2CH=CH_2$), 228, 169, 143, 101, 41 (bp); CIMS (isobutane): 285 (M^++H); HRMS (M^++H) calculated for $C_{17}H_{33}O_3$: 285.2428. Found 285.2448.

$[\alpha]_D^{20}$+6.48° (*c* 1.11, $CHCl_3$).

4.8. Methyl (*S*)-3-(2-hydroxyethyl)oxytridecanoate

Ozone was introduced into a stirred solution of methyl (*S*)-3-allyloxytridecanoate (916 mg, 3.22 mmol) in methanol (100 ml) at −60∼−50°C for 75 min. After bubbling of argon, dimethylsulfide (2.0 ml, 27.2 mmol) was added at the same temperature, and the mixture was warmed to 23°C over 3 h. Stirring was continued for an additional 1 h at the same temperature, then the solvent was removed. The residue was dissolved in methanol (12.0 ml), and sodium borohydride (125.6 mg, 3.32 mmol) was added at 0°C. More sodium borohydride (61.4 mg, 63.1 mg, and 125.6 mg, respectively) was added after stirring at 0°C for 0.5, 1 and 1.5 h. After addition of water the pH of the reaction mixture was adjusted to 5 with 1 N aqueous HCl, and the solution was ex-

tracted with $CHCl_3$. The organic layer was washed with brine, dried (Na_2SO_4), and concentrated. The residue was purified by silica gel column chromatography (hexane-AcOEt, 5:1–3:1) to give methyl (*S*)-3-(2-hydroxyethyl)oxytridecanoate (862 mg, 93%) as a colorless oil.

^{1}H-NMR ($CDCl_3$, 500 MHz) δ 0.88 (t, J = 6.9 Hz, 3H), 1.29 (m, 16H), 1.53 (m, 2H), 2.48 (dd, J = 4.7, 15.6 Hz, 1H), 2.53 (dd, J = 7.9, 15.6 Hz, 1H), 2.59 (bs, 1H), 3.55 (m, 1H), 3.63–3.70 (m, 3H), 3.70 (s, 3H), 3.81 (m, 1H); ^{13}C-NMR ($CDCl_3$, 125 MHz) δ 14.10, 22.69, 25.14, 29.33, 29.57, 29.59, 29.61, 29.68, 31.92, 34.10, 39.42, 51.76, 62.08, 70.55, 76.44, 172.23; IR (neat) 3475, 2930, 2860, 1740, 1440, 1115, 1060 cm^{-1}; MS *m/z* 257 (M^+-OMe), 243 (M^+-CH_2CH_2OH), 228, 169, 147, 73 (bp); CIMS (isobutane): 289 (M^++H); HRMS (M^+-OMe) calculated for $C_{15}H_{29}O_3$: 257.2115. Found 257.2117.

$[\alpha]_D^{20}$+18.18° (*c* 0.495, $CHCl_3$).

4.9. (S)-3-(2-Hydroxyethyl)oxytridecanoic acid

To a solution of methyl (*S*)-3-(2-hydroxyethyl)oxytridecanoate (751.1 mg, 2.48 mmol) in methanol (14 ml) was added 1 N aqueous NaOH (7.0 ml, 7.0 mmol) at 0°C, and the mixture was stirred at 23°C for 3 h. The reaction mixture was acidified to pH 3 with 1 N aqueous HCl, followed by extraction with CH_2Cl_2. The combined organic layers were washed with water and brine, dried (Na_2SO_4), and concentrated to afford (*S*)-3-(2-hydroxyethyl)oxytridecanoic acid (667.3 mg, 98%) as a colorless solid.

^{1}H-NMR ($CDCl_3$, 500 MHz) δ 0.88 (t, J = 6.9 Hz, 3H), 1.26 (m, 16H), 1.50 (m, 1H), 1.62 (m, 1H), 2.52 (dd, J = 7.6, 15.8 Hz, 1H), 2.56 (dd, J = 4.8, 15.8 Hz, 1H), 3.08 (broad), 3.56 (m, 1H), 3.68–3.75 (m, 3H), 3.80 (m, 1H); ^{13}C-NMR ($CDCl_3$, 125 MHz) δ 14.07, 22.65, 25.09, 29.29, 29.52, 29.55, 29.57, 29.62, 31.87, 33.92, 39.29, 61.84, 70.43, 76.52, 176.27; IR (neat) 3400, 2930, 2860, 1720, 1465, 1110, 1060 cm^{-1}; MS *m/z* 257 (M^+-OH), 243 (M^+-CH_2OH), 229 (M^+-CH_2CH_2OH), 213, 169, 133, 115, 86, 73 (bp); CIMS (isobutane): 275 (M^++H); HRMS (M^+-OH) calculated for $C_{15}H_{29}O_3$: 257.2115. Found 257.2129.

$[\alpha]_D^{20}$+16.76° (*c* 0.525, $CHCl_3$); mp 33–34°C.

4.10. tert-Butyldiphenylsilyl (S)-3-(2-tert-butyldiphenylsilyloxyethyl)oxytridecanoate

To a solution of (*S*)-3-(2-hydroxyethyl)oxytridecanoic Acid (687.4 mg, 2.51 mmol) and imidazole (682.3 mg, 10.1 mmol) in DMF (3.5 ml) was added *tert*-butyldiphenylsilyl chloride (1.83 ml, 7.04 mmol) at 0°C, and the mixture was stirred at 23°C for 2 h. After addition of water the mixture was extracted with Et_2O. The organic layer was washed with water, dried (Na_2SO_4), and concentrated. The residue was purified by silica gel column chromatography (hexane-AcOEt, 30:1) to give *tert*-butyldiphenylsilyl (*S*)-3-(2-*tert*-butyldiphenylsilyloxyethyl)oxytridecanoate (1.737 g, 92%) as a colorless oil.

^{1}H-NMR ($CDCl_3$, 500 MHz) δ 0.88 (t, J = 7.0 Hz, 3H), 1.04 (s, 9H), 1.08 (s, 9H), 1.25 (m, 16H), 1.39 (m, 1H), 1.51 (m, 1H), 2.55 (dd, J = 5.8, 15.5 Hz, 1H), 2.71 (dd, J = 6.9, 15.5 Hz, 1H), 3.56 (t, J = 5.2 Hz, 2H), 3.69–3.81 (m, 3H), 7.36 (m, 12H), 7.67 (m, 8H); ^{13}C-NMR ($CDCl_3$, 125 MHz) δ 14.12, 19.10, 19.19, 22.69, 25.22, 26.83, 26.93, 29.34, 29.61, 29.63, 29.65, 29.78, 31.93, 34.42, 41.60, 63.46, 70.51, 76.75, 127.61, 127.63, 127.64, 127.66, 129.56, 130.00, 131.86, 131.89, 133.77, 133.82, 135.32, 135.33, 135.62, 135.64, 171.09; IR (neat) 2930, 2860, 1730, 1430, 1115, 700, 505 cm^{-1}; MS *m/z* 693 (M^+-^{t}Bu), 481, 425, 393 (bp), 373, 213, 199, 135; CIMS (isobutane): 751 (M^++H); Anal. calculated for $C_{47}H_{66}O_4Si_2$: C 75.15, H 8.86. Found C 74.87, H 8.89.

$[\alpha]_D^{20}$+1.04° (*c* 0.960, $CHCl_3$).

4.11. (S)-3-(2-tert-Butyldiphenylsilyloxyethyl)oxytridecanoic acid (**11**)

To a solution of *tert*-butyldiphenylsilyl (*S*)-3-(2-*tert*-butyldiphenylsilyloxyethyl)oxytridecanoate (1.682 g, 2.24 mmol) in THF (22.4 ml) were added methanol (33.5 ml) and an aqueous solution of K_2CO_3 (929.0 mg, 6.72 mmol in 11.2 ml), and the mixture was stirred at 23°C for 1 h. After removal of organic solvent by evaporation brine was added, and the mixture was acidified to pH 2–3 with 1 M $KHSO_4$, followed by extraction with Et_2O. The organic layer was washed with brine, dried (Na_2SO_4), and concentrated. The residue was purified by silica gel column chromatography ($CHCl_3$–MeOH, 100:1) to give **11** (1.068 g, 93%) as a colorless oil.

^{1}H-NMR ($CDCl_3$, 500 MHz) δ 0.88 (t, J = 6.9 Hz, 3H), 1.05 (s, 9H), 1.25 (m, 16H), 1.52 (m, 1H), 1.63 (m, 1H), 2.54 (dd, J = 6.9, 15.8 Hz, 1H), 2.61 (dd, J = 4.4, 15.8 Hz, 1H), 3.60 (m, 1H), 3.65 (m, 1H), 3.74 (m, 2H), 3.81 (m, 1H), 7.41 (m, 6H), 7.67 (m, 4H), 9.65, (bs, 1H); ^{13}C-NMR ($CDCl_3$, 125 MHz) δ 14.09, 19.11, 22.66, 25.00, 26.77, 29.30, 29.53, 29.57, 29.58, 29.62, 31.89, 33.93, 39.07, 63.28, 70.53, 76.34, 127.65, 129.65, 133.48, 135.61, 175.32; IR (neat) 2930, 2860, 1710, 1430, 1110, 705, 505 cm^{-1}; MS *m/z* 495 (M^+-OH), 455 (M^+-^{t}Bu), 437, 377, 299, 243, 199, 165 (bp); HRMS (M^+-OH) calculated for $C_{31}H_{47}O_3Si$: 495.3291. Found 495.3262.

$[\alpha]_D^{20}$+5.74° (*c* 0.940, $CHCl_3$).

4.12. (R)-5-[(S)-3-(2-tert-Butyldiphenylsilyloxyethyl)-oxytridecanoyl]oxymethyl-4-hydroxy-3-hexadecanoylfuran-2-(5H)-one (**12**)

To a solution of **11** (324 mg, 0.632 mmol) in CH_2Cl_2 (2.2 ml) were added DMF (2 drops) and oxalyl chloride (0.22 ml, 2.52 mmol) at 0°C, and the mixture was stirred at 23°C for 16 h. After evaporation of the volatile materials, the residue was redissolved in CH_2Cl_2. To this solution was added a solution of **1** (465.8 mg, 1.264 mmol) in CH_2Cl_2 (22.0 ml), and then pyridine (80.92 ml, 11.37 mmol) was added at 0°C. The mixture was stirred at 23°C for 48 h, and quenched by the addition of saturated aqueous $NaHCO_3$. The mixture was acidified to pH 4 with 0.5 N aqueous HCl, followed by extraction with CH_2Cl_2. The organic layer was dried (Na_2SO_4), and concentrated. The residue was purified by silica gel column chromatography (hexane-AcOEt, 1:0–0:1, and then $CHCl_3$–MeOH, 5:1–3:1) to give **12** (485.1 mg, 89%) as a pale yellow oil, and **1** (69.6 mg) was recovered from the fraction eluted with $CHCl_3$–MeOH.

^{1}H-NMR ($CDCl_3$, 500 MHz) δ 0.88 (t, J = 6.9 Hz, 6H), 1.04 (s, 9H), 1.25 (m, 40H), 1.49 (m, 2H), 1.69 (m, 2H), 2.40 (m, 1H), 2.61 (m, 1H), 2.9 (m, 2H), 3.54 (m, 2H), 3.69 (m, 1H), 3.74 (m, 2H), 4.30 (m, 1H), 4.56 (dd, J = 3.0, 12.4 Hz, 1H), 4.76 (dd, J = 2.8, 4.6 Hz, 0.5H), 4.87 (dd, J = 3.2, 4.4Hz, 0.5H), 7.39 (m, 6H), 7.68 (m, 4H); IR (neat) 3460, 2920, 2850, 1745, 1695, 1600, 1460, 1110, 700 cm^{-1}; MS *m/z* 693, 373, 350, 299, 243, 199 (bp), 165; CIMS (isobutane): 861 (M^++H), 805 (M^+-^{t}Bu), 785 (M^+-Ph); HR-FABMS (glycerol:nitrobenzylalcohol = 1:2,

+NaCl) (M^++Na) calculated for $C_{52}H_{82}O_8SiNa$: 885.5677. Found 885.5687.

4.13. *(R)-5-[(S)-3-(2-Hydroxyethyl)oxytridecanoyl]oxymethyl-4-hydroxy-3-hexadecanoylfuran-2-(5H)-one (**13**)*

To a solution of **12** (342.5 mg, 0.397 mmol) in THF (10.0 ml) was added TBAF (1 M THF solution, 0.67 ml, 0.67 mmol), and the mixture was stirred at 23°C for 5 h. The reaction mixture was quenched by the addition of saturated aqueous NH_4Cl and then extracted with Et_2O. The organic layer was washed with brine, dried (Na_2SO_4), and concentrated. The residue was purified by silica gel thin layer chromatography ($CHCl_3$–MeOH, 10:1) and following 0.5 N aqueous HCl treatment to give **13** (180.2 mg, 73%) as a pale yellow amorphous solid.

^{1}H-NMR ($CDCl_3$, 500 MHz) δ 0.88 (t, J = 6.9 Hz, 6H), 1.26 (m, 38H), 1.41 (m, 3H), 1.56 (m, 1H), 1.71 (m, 2H), 2.47 (d, J = 5.2 Hz, 2H), 2.93 (br t, J = 7.4 Hz, 2H), 3.51 (m, 1H), 3.62 (m, 1H), 3.67 (m, 2H), 3.74 (m, 1H), 4.42 (m, 1H), 4.58 (m, 1H), 4.81 (br s, 0.5H), 4.92 (br s, 0.5H); ^{13}C-NMR ($CDCl_3$, 125 MHz) δ 14.12, 22.69, 22.70, 25.15, 29.24, 29.34, 29.37, 29.43, 29.59, 29.60, 29.62, 29.67, 29.69, 29.71, 29.72, 31.92, 31.94, 33.97, 39.31, 61.82, 62.04, 70.57, 76.29, 77.25, 171.38 (carbonyl carbons of the tetronic acid group were not observed in $CDCl_3$ due to tautomeric isomerization); IR (neat) 3500, 2910, 2840, 1740, 1690, 1600, 1460 cm^{-1}; MS *m/z* 606 (M^+-H_2O), 350, 154, 115, 86 (bp), 73; CIMS (isobutane): 625 (M^++H), 607 (M^+-OH); HR-FABMS (glycerol:nitrobenzylalcohol = 1:2, +NaCl) (M^++ Na) calculated for $C_{36}H_{64}O_8Na$: 647.4499. Found 647.4476.

$[\alpha]_D^{20}$+39.79° (*c* 0.960, $CHCl_3$).

4.14. *(R)-5-[(3S,12R)-3-Decyl-12-methoxycarbonyl-4,7,11-trioxa-8,10-dioxo-13-(triphenylmethyoxy)tetradecanoyl] oxymethyl-3-hexadecanoyl-4-hydroxyfuran-2-(5H)-one (**15**)*

To a solution of **13** (71.3 mg, 0.0676 mmol) and **14** (127.7 mg, 0.245 mmol) in benzene (60.0 ml) were added Na_2HPO_4 (208.7 mg, 1.470 mmol) and silver trifluoroacetate (170.3 mg, 0.771 mmol), and the mixture was stirred at 23°C for 5 h while shielded from light. Then it was refluxed for 30 min without shielding from light. The resulting black insoluble material was removed by filtration through a Celite pad, and the filtrate was concentrated. The residue was purified by silica gel column chromatography ($CHCl_3$–MeOH, 15:1) followed by 0.5 N aqueous HCl treatment to give **15** (98.1 mg, 60%) as a colorless oil. A mixture fraction containing **16** (64 mg) was also obtained.

^{1}H-NMR ($CDCl_3$, 500 MHz) δ 0.88 (m, 6H), 1.25 (m, 38H), 1.38 (m, 3H), 1.50 (m, 1H), 1.69 (m, 2H), 2.44 (m, 2H), 2.91 (m, 2H), 3.50 (d, J = 4.1 Hz, 2H), 3.58 (s, 2H), 3.65 (m, 3H), 3.73 (s, 3H), 4.23 (m, 2H), 4.35 (m, 1H), 4.58 (m, 1H), 4.78 (dd, J = 2.8, 4.6 Hz, 0.5H), 4.88 (dd, J = 3.2, 4.2 Hz, 0.5H), 5.27 (m, 1H), 7.24 (m, 3H), 7.30 (t, J = 7.5 Hz, 6H), 7.41 (d, J = 7.5 Hz, 6H); IR (neat) 3480, 2920, 2850, 1740, 1695, 1600, 1450, 1095, 705 cm^{-1}; FABMS (glycerol:nitrobenzylalcohol = 1:2, +NaCl) *m/z* 1099 (M^+-H+2Na), 1077 (M^++Na), 857, 835, 243 (bp); HR-FABMS (glycerol:nitrobenzylalcohol = 1:2, +NaCl) (M^++Na) calculated for $C_{62}H_{86}O_{14}Na$: 1077.5915. Found 1077.5924.

4.15. *(R)-5-{3(S)-Decyl-6-[2,5-dihydro-4-hydroxy-5(R)-hydroxymethyl-2-oxofuran-3-yl]carbonyloxy-4-oxahexanoyl} oxymethyl-3-hexadecanoyl-4-hydroxyfuran-2-(5H)-one (**8**)*

To a solution of **15** (71.3 mg, 0.0676 mmol) in THF (1.2 ml) was added TBAF (1 M THF solution, 0.14 ml, 0.14 mmol), and the mixture was stirred at 23°C for 31 h. During the reaction TBAF (0.14 ml after 17 h, and 0.07 ml after 25 h) was further added to complete the reaction. The reaction mixture was acidified to pH 3 with 0.5 N aqueous HCl and poured into ice-water; the mixture was then extracted with Et_2O. The combined organic layers were washed with brine, dried (Na_2SO_4), and concentrated. The residue was purified by silica gel column chromatography ($CHCl_3$–MeOH, 10:1) and following 0.5 N aqueous HCl treatment to give (*R*)-5-{3(*S*)-decyl-6-[2,5-dihydro-4-hydroxy-2-oxo-5(*R*)-(triphenylmethyloxymethyl)furan-3-yl]carbonyloxy-4-oxahexanoyl}oxymethyl-3-hexadecanoyl-4-hydroxyfuran-2-(5*H*)-one (38.5 mg, 73%) as a pale yellow oil.

^{1}H-NMR ($CDCl_3$, 500 MHz) δ 0.88 (m, 6H), 1.25 (m, 38H), 1.39 (m, 3H), 1.55 (m, 1H), 1.66 (m, 2H), 2.47 (m, 2H), 2.91 (m, 2H), 3.41 (dd, J = 4.1, 10.5 Hz, 1H), 3.66 (dd, J = 3.0, 10.5 Hz, 1H), 3.78 (m, 3H), 4.38 (m, 2H), 4.48 (m, 1H), 4.77 (br s, 0.5H), 4.87 (br s, 0.5H), 4.93 (br s, 1H), 7.20–7.33 (m, 9H), 7.39 (d, J = 7.5 Hz, 6H); IR (neat) 2920, 2850, 1770, 1740, 1695, 1640, 1600, 1465, 1060, 705 cm^{-1}; FABMS (glycerol:nitrobenzylalcohol = 1:2, +NaCl) *m/z* 1089 (M^+-2H+3Na), 669, 647, 243 (bp); HR-FABMS (glycerol:nitrobenzylalcohol = 1:2, +NaCl) (M^+-2H+3Na) calculated for $C_{61}H_{80}O_{13}Na_3$: 1089.5292. Found 1089.5255.

To a solution of (*R*)-5-{3(*S*)-decyl-6-[2,5-dihydro-4-hydroxy-2-oxo-5(*R*)-(triphenylmethyloxymethyl)furan-3-yl]carbonyloxy-4-oxahexanoyl}oxymethyl-3-hexadecanoyl-4-hydroxyfuran-2-(5*H*)-one (51.6 mg, 0.0504 mmol) in methanol (1.5 ml) was added 1 N aqueous HCl (0.10 ml, 0.10 mmol), and the mixture was stirred at 23°C for 6 h. After removal of the solvent in vacuo, the residue was purified by silica gel thin layer chromatography ($CHCl_3$–MeOH, 5:1) and following 0.5 N aqueous HCl treatment to give **8** (32.2 mg, 82%) as a colorless amorphous solid.

^{1}H-NMR ($CDCl_3$, 500 MHz) δ 0.88 (t, J = 6.9 Hz, 6H), 1.29 (m, 38H), 1.41 (m, 3H), 1.55 (m, 1H), 1.70 (m, 2H), 2.45 (dd, J = 4.5, 15.7 Hz, 1H), 2.50 (dd, J = 7.8, 15.7 Hz, 1H), 2.92 (m, 2H), 3.77 (m, 3H), 3.98 (dd, J = 3.2, 12.5 Hz, 1H), 4.13 (dd, J = 2.3, 12.5 Hz, 1H), 4.38 (m, 2H), 4.48 (m, 1H), 4.58 (dd, J = 2.8, 12.5 Hz, 1H), 4.89 (br s, 1H), 4.94 (br s, 1H); ^{13}C-NMR (CD_3OD, 125 MHz) δ 14.48, 14.50, 23.76, 23.78, 26.30, 30.50, 30.53, 30.65, 30.80, 30.82, 30.83, 33.13, 35.31, 40.44, 61.31, 63.10, 64.65, 68.35, 78.14, 80.47, 80.88, 95.31, 100.22, 163.58, 172.09, 172.32, 173.51, 188.11, 194.72, 195.92; IR (neat) 3450, 2920, 2850, 1770, 1740, 1690, 1650, 1465, 1050 cm^{-1}; FABMS (glycerol:nitrobenzylalcohol = 1:1, +NaCl) *m/z* 825 (M^+-H+2Na), 803 (M^++Na), 781 (M^++H), 669, 647, 242 (bp); HR-FABMS (glycerol:nitrobenzylalcohol = 1:2, +NaCl) (M^++Na) calculated for $C_{42}H_{68}O_{13}Na$: 803.4558. Found 803.4550.

$[\alpha]_D^{20}$+40.41° (*c* 0.480, $CHCl_3$).

Crude mixture containing **16** was also converted to **8** as follows. To a solution of **16** (37.3 mg, maximum 0.0356 mmol) in THF (0.8 ml) was added TBAF (1 M THF solution, 0.095 ml, 0.095 mmol), and the mixture was stirred at 23°C for 22 h. During the reaction TBAF (0.19 ml) was further added after 6 h to

complete the reaction. The reaction mixture was acidified to pH 3 with 0.5 N aqueous HCl and poured into ice-water; the mixture was then extracted with Et_2O and Et_2O-methanol = 1:1. The combined organic layers was washed with brine, dried (Na_2SO_4), and concentrated. The residue was purified by silica gel thin layer chromatography ($CHCl_3$–MeOH, 5:1) and following 0.5 N aqueous HCl treatment to give **8** (19.1 mg, 69%〜) as a pale yellow oil.

4.16. Binding model of VHR-(RK-682)$_2$ complex

The 3D structure of the complex of VHR and two RK-682 molecules was estimated through energy minimization and dynamics simulation. The initial structure was generated by docking two RK-682 molecules to a VHR molecule manually, considering the putative binding site and the interaction energy in a vacuum, using the computer program Hyper-Chem (Hypercube Inc., Canada). The 3D structure of the VHR molecule based on X-ray crystallography has already been reported [5] and was used in the present study as the initial structure. For energy minimization and analysis of the molecular dynamics in water, we used the Amber 4.1 computer package (Pearlman, DA, Case DA, Caldwall JW, Amber 4.1 1995; UCSF, San Francisco, CA) and a Spark Station 5 workstation (Sun Inc., USA) with a specially designed board, the MD-engine (Fuji-Xerox, Japan), for molecular dynamics calculation. The initial structure of the complex was solvated with 3711 TIP3P water molecules, using a protein box size of $5.9\times5.0\times4.1$ nm^3. The minimum thickness of the solvent shell was 0.6 nm. We basically followed the Ewald method to treat the electrostatics, using a 0.6 nm cutoff, a 1 fs time step and constant volume with periodic boundary conditions. The non-bonded pair list was updated every 20 steps. The energy of the solvated structure was minimized with 100 steps. The molecular dynamics simulation was done from the energy-minimized structure. At first, the temperature in the simulation was increased rapidly from 0 K to 400 K in 10 K steps with a 0.1 ps calculation for each of the steps. The temperature of the system was controlled by Berendsen's algorithm with a 0.2 ps coupling constant. After the scanning, a constant temperature simulation was done at 310 K for 10 ps. Finally the temperature of the system was decreased slowly from 310 K to 0 K in 1 K steps, with a 0.1 ps simulation for each step. The total energy of the final structure was substantially lower than that of the energy-minimized structure.

Acknowledgements

We thank Dr. M. Nishiyama and Dr. H. Ohmori for a useful discussion about steady-state kinetics. We also thank Dr. N. Morisaki and Dr. Y. Hashimoto (University of Tokyo) for measuring HR-FAB mass spectra. This work was supported in part by a grant for Multibioprobe (RIKEN), by a Grant-in-Aid from the Ministry of Education, Science, Sports and Culture (T.U. and H.O.), and by grants from the Hayashi Memorial Foundation for Female Natural Scientists, the Kato Memorial Bioscience Foundation, and the Mochida Memorial Foundation for Medicinal and Pharmaceutical Research (M.S.).

References

[1] E.B. Fauman, M.A. Saper, Structure and function of the protein tyrosine phosphatases, Trends Biochem. Sci. 21 (1996) 413–417.
[2] N.K. Tonks, B.G. Neel, From form to function signaling by protein tyrosine phosphatases, Cell 87 (1996) 365–368.
[3] J.M. Denu, J.A. Stuckey, M.A. Saper, J.E. Dixon, Form and function in protein dephosphorylation, Cell 87 (1996) 361–364.
[4] T. Ishibashi, D.P. Bottaro, A. Chan, T. Miki, S.A. Aaronson, Expression cloning of a human dual-specificity phosphatase, Proc. Natl. Acad. Sci. USA 89 (1992) 12170–12174.
[5] J. Yuvaniyama, J.M. Denu, J.E. Dixon, M.A. Saper, Crystal structure of the dual specificity protein phosphatase VHR, Science 272 (1996) 1328–1331.
[6] J.L. Todd, K.G. Tanner, J.M. Denu, Extracellular regulated kinases (ERK)1 and ERK2 are authentic substrates for the dual-specificity protein-tyrosine phosphatase VHR, J. Biol. Chem. 274 (1999) 13271–13280.
[7] T. Hamaguchi, T. Sudo, H. Osada, RK-682, a potent inhibitor of tyrosine phosphatase, arrested the mammalian cell cycle progression at G_1 phase, FEBS Lett. 372 (1995) 54–58.
[8] T. Hamaguchi, A. Masuda, T. Morino, H. Osada, Stevastelins, a novel group of immunosuppressants, inhibit dual-specificity protein phosphatases, Chem. Biol. 4 (1997) 279–286.
[9] T. Hamaguchi, A. Takahashi, T. Kagamizono, A. Manaka, M. Sato, H. Osada, Synthesis and characterization of a potent and selective protein tyrosine phosphatase inhibitor, 2-[(4-methylthiopyridin-2-yl)-methylsulfinyl]benzimidazole, Bioorg. Med. Chem. Lett. 10 (2000) 2657–2660.
[10] G. Bergnes, C.L. Gilliam, M.D. Boisclair, J.L. Blanchard, K.V. Blake, D.M. Epstein, K. Pal, Generation of an Ugi Library of phosphate mimic-containing compounds and identification of novel dual specific phosphatase inhibitors, Bioorg. Med. Chem. Lett. 9 (1999) 2849–2854.
[11] M.S. Malamas, J. Sredy, C. Moxham, A. Katz, W. Xu, R. McDevitt, F.O. Adebayo, D.R. Sawicki, L. Seestaller, D. Sullivan, J.R. Taylor, Novel benzofuran and benzothiophene biphenyls as inhibitors of protein tyrosine phosphatase 1B with antihyperglycemic properties, J. Med. Chem. 43 (2000) 1293–1310.
[12] S. Shinagawa, M. Muroi, R. Itoh, Jpn Kokai Tokkyo Koho (1993) JP 05-43568.
[13] B.E. Roggo, F. Petersen, R. Delmendo, H.B. Jenny, H.H. Peter, J. Roesel, 3-Alkanoyl-5-hydroxymethyl tetronic acid homologues and resistomysin: new inhibitors of HIV-1 Protease I. Fermentation, isolation, and biological activity, J. Antibiot. 47 (1994) 136–142.
[14] B.E. Roggo, P. Hug, S. Moss, F. Raschdorf, H.H. Peter, 3-Alkanoyl-5-hydroxymethyl tetronic acid homologues and resistomysin: new inhibitors of HIV-1 Protease II. structure determination, J. Antibiot. 47 (1994) 143–147.
[15] M. Sodeoka, R. Sampe, T. Kagamizono, H. Osada, Asymmetric synthesis of RK-682 and its analogs, and evaluation of their protein phosphatase inhibitory activity, Tetrahedron Lett. 37 (1996) 8775–8778.
[16] M. Sodeoka, R. Sampe, S. Kojima, Y. Baba, N. Morisaki, Y. Hashimoto, Asymmetric synthesis of a 3-acyltetronic acid derivative, RK-682, and formation of its calcium salt during silica gel column chromatography, Chem. Pharm. Bull. 49 (2001) 206–212.
[17] M. Sodeoka, R. Sampe, S. Kojima, Y. Baba, T. Usui, K. Ueda, H. Osada, Synthesis of a tetronic acid library focused on inhibitors of tyrosine and dual-specificity protein phosphatases and its evaluation regarding VHR and Cdc25B inhibition, J. Med. Chem. (2001) 3216–3222.
[18] R. Noyori, M. Ohkuma, H. Kitamura, N. Takaya, H. Sayo, H. Kumobayashi, S. Akutagawa, Asymmetric hydrogenation of β-keto carboxylic esters. A practical, purely chemical access to β-hydroxy

esters in high enantiomeric purity, J. Am. Chem. Soc. 109 (1987) 5856–5858.

[19] Y.A. Puius, Y. Zhao, M. Sullivan, D.S. Lawrence, S.C. Almo, Z.Y. Zhang, Identification of a second aryl phosphate-binding site in protein-tyrosine phosphatase 1B: A paradigm for inhibitor design, Proc. Natl. Acad. Sci. USA 94 (1997) 13420–13425.

[20] M. Taing, Y.F. Keng, K. Shen, L. Wu, D.S. Lawrence, Z.Y. Zhang, Potent and highly selective inhibitors of the protein tyrosine phosphatase 1B, Biochemistry 38 (1999) 3793–3803.

[21] R.S. Reddy, G. Swarup, Alternative splicing generates four different forms of a non-transmembrane protein tyrosine phosphatase mRNA, DNA Cell Biol. 14 (1995) 1007–1015.

[22] J.M. Denu, G. Zhou, L. Wu, R. Zhao, J. Yuvaniyama, M.A. Saper, J.E. Dixon, The purification and characterization of a human dual-specific protein tyrosine phosphatase, J. Biol. Chem. 270 (1995) 3796–3803.

[23] T. Usui, G. Marriott, M. Inagaki, G. Swarup, H. Osada, Protein phosphatase 2A inhibitors, phoslactomycins. Effects on the cytoskeleton in NIH/3T3 cells, J. Biochem. 125 (1999) 960–965.